Nonlinear Landau Damping of Purely Perpendicular Bernstein Modes

Spilios Riyopoulos
Institute for Fusion Studies
The University of Texas at Austin
Austin, Texas 78712-1060

Abstract

The linear dispersion relation for Bernstein modes, obtained by the integration of Vlasov's equation along the unperturbed cyclotron orbits, predicts that the modes propagating perpendicularly to the magnetic field are undamped, i.e., $\gamma_L \to 0$ as $k_{||} \to 0$. However, when ω is close to a resonance $\omega_n = n\Omega_c$, most of the particles become trapped for small wave amplitude E and the unperturbed orbit approximation breaks down. The trapped particle trajectories are calculated analytically here using a resonant Hamiltonian approximation. Integration, consistent with the wave, along the orbits yields the nonlinear damping rate in a similar manner as the one used by O'Neil (1965) for the damping of unmagnetized electrostatic modes. The results can be extended for the general case of almost perpendicular, short wavelength electrostatic modes near cyclotron harmonics.

I. Introduction

The linear dispersion relation for Bernstein modes, obtained by the integration of Vlasov's equation over unperturbed cyclotron orbits is expressed by

$$\text{Re } \varepsilon(k,\omega) = 1 - \sum_a \frac{\omega_{pa}^2}{k_\perp^2 v_\perp^2} \sum_{n=1}^{\infty} \frac{2n^2\Omega_{ca}^2}{\omega^2 - n^2\Omega_{ca}^2} I_n^2(k_\perp^2\rho_L^2) e^{-k_\perp^2\rho_L^2} = 0 \qquad (1a)$$

$$\text{Im } \varepsilon(k,\omega) \cong \pi \frac{\omega_{pa}^2}{k_\perp^2 v_\perp^2} I_0(k_\perp^2\rho_L) e^{-k_\perp^2\rho_L^2} \left(\frac{\omega - \omega_{ca}}{k_\parallel v_\parallel}\right) e^{-\left(\frac{\omega - \Omega_{ca}}{k_\parallel v_\parallel}\right)^2} \qquad (1b)$$

$$\gamma_L = \text{Im}(\omega) = -\frac{\text{Im}(\varepsilon)}{\frac{\partial}{\partial\omega}\text{Re}(\omega)}\Big|_{\omega_r} \quad , \quad k_\parallel \ll k_\perp \qquad (1c)$$

where subscript a signifies either electrons or ions and ω_{pa}, Ω_{ca} are the corresponding plasma and cyclotron frequencies. Equation (1a) describes short wavelength ($k\rho_L$ can be $>$ 1 for $\omega_{pa} \gg \Omega_{ca}$) electrostatic modes propagating almost perpendicularly to the magnetic field. Equation (1c) shows that the damping rate is extremely small for $k_\parallel \ll (\omega - n\Omega_{ca})/v_{th}$ and that the purely perpendicular modes are undamped, since $\gamma_L \equiv \text{Im}(\omega) \to 0$ for $k_\parallel \to 0$. This is due to the fact that the wave particle resonances responsible for the damping occur in the linear theory when the Doppler shifted wave frequency sensed by a free streaming particle along the magnetic lines matches a cyclotron harmonic, $\omega - k_\parallel v_\parallel = n\Omega_{ca}$. For $(\omega - n\Omega_{ca})/k_\parallel \gg v_{th}$ there are only a few resonant particles and their number vanishes at the limit $k_\parallel \to 0$. However, for ω in the vicinity of a cyclotron harmonic $n\Omega_{ca}$ and $k_\parallel \ll k_\perp$, a nonlinear trapping mechanism is activated (Fukuyama et al., 1977; Karney 1979) which completely changes the character of the motion. This nonlinear trapping can be conceived as an oscillation of the perpendicular velocity $v_\perp$ due to a sequence of correlated kicks $\Delta v_\perp$ received from the wave over the time span of many gyroperiods. This is shown in Figs. 1 and 2 where we have trapped particle motion for small wave amplitude with wave frequency equal and close to the second cyclotron harmonic respectively. In Fig. 3, the wave frequency is "far" from resonance and particles execute trajectories very similar to the unperturbed cyclotron orbits used in the linear theory. The main objective in this paper is to obtain the nonlinear damping rate utilizing the consistent with the wave trajectories in a similar manner used by O'Neil (1965) for the damping of unmagnetized

electrostatic modes. The analysis can be easily generalized to include any perpendicularly propagating electrostatic mode near a cyclotron harmonic, such as, for example, the fast magnetosonic wave near the ion-ion hybrid resonance in a two species plasma with small minority concentration. In short, the nonlinear effects produce a direct coupling of the wave energy to the ions and therefore the results obtained here can apply to ion cyclotron plasma heating. In Sec. II, the analytic solutions for the particle trajectories are obtained using a resonant Hamiltonian approximation. In Sec. III, the time evolution of the velocity distribution function along such orbits is determined and energy balance between the wave electrostatic energy and the particles kinetic energy yields the damping rate. Section IV contains a more detailed discussion and comparisons with numerical results obtained performing particle code simulations.

II. Calculation of the Trajectories

Assuming for simplicity that $k_{\|} = 0$, the Hamiltonian of a particle in a uniform magnetic field $B = B_0\hat{z}$ under the influence of a perpendicular electrostatic wave $\mathbf{E} = \hat{y}E_0\cos(k_\perp y - \omega t)$ is given in normalized units (time to Ω_c^{-1}, length to $k_\perp^{-1}$) by

$$H(P_y, y) = \frac{1}{2}(P_y^2 + y^2) - \alpha\sin(y + Y - \nu t) \tag{2a}$$

with $\alpha = (2eE_0/k_\perp)/m(\Omega_c/k_\perp)^2$, $\nu = \omega/\Omega_c$, and $\Omega_c = eB_0/(mc)$. Here P_x and P_y are the canonical momentum components expressed in the normalized units by $P_y = p_y$, $P_x = p_x - y$ and (x, y) signify the position relative to the guiding center coordinates (X, Y). P_x coincides with the position of the guiding center Y and is a constant of the motion because H does not depend on x. This is utilized by shifting the origin of our coordinate system onto the guiding center position, yielding $P_x = 0$ and reducing the original two dimensional Hamiltonian (for example Eq. (4) obtained by Karney (1978)) to the one dimensional result, Eq. (2a). The transformation $y = (2I)^{1/2}\sin\vartheta_1$, $P_y = (2I)^{1/2}\cos\vartheta_1$, $\vartheta_2 = \nu t$, $K = -E/\nu$ transforms the Hamiltonian into

$$H = I + \nu K - \alpha\sum_{m=-\infty}^{\infty} J_m(r)\sin(m\vartheta_1 - \vartheta_2 + Y),$$

with

$$r = (2I)^{1/2} = (k_\perp v_\perp / \Omega_c).$$

To the lowest order $\dot{\vartheta}_1 = 1$, $\dot{\vartheta}_2 = \nu$, and since in the case of interest ν is close to n (i.e., $\omega \cong n\Omega_c$) the main contribution comes from the resonant term $m = n \equiv \mathrm{Int}(\nu)$,

$$H_R \cong I + \nu K - \alpha J_n(r) \sin(n\vartheta_1 - \vartheta_2 + Y).$$

For low harmonics (small n) one can approximate $J_n(r)$ by $J_n(r) \cong (2/\pi r)^{1/2} \cos[r - (n + 1/2)\pi/2]$ provided that $r > 4n^2/8$. Now, a local approximation of H_R around the zeros r_i of $J_n'(r_i) = 0$ is performed, as it will be soon clear that these points signify the location of the centers of the trapped particle islands in phase space. From the above representation for the Bessel functions it is found that $r_i \cong i\pi + (n + 1/2)\pi/2$, i=integer, and one can approximate $r = \sqrt{2I}$ by $r \cong r_i + (I - I_i)/r_i$, for $|r - r_i| \leq \pi/2 < r_i$. Defining new canonical coordinates

$$J_\psi = (I - I_i)/r_i,$$

$$\psi = n\vartheta_1 - \vartheta_2 + (Y - \pi/2) + i\pi,$$

$$J_\phi = n/r_i K + (I - I_i)/r_i,$$

$$\phi = \vartheta_2 - (Y - \pi/2) - i\pi,$$

and rescaling H_R leads to

$$H_i = -\delta J_\psi + \nu J_\varphi - A_i \cos J_\psi \cos\psi \qquad (2b)$$

with $A_i = \alpha n / r_i (2/\pi r_i)^{1/2}$, $\delta = \nu - n$.

The above procedure is analogous to the one followed by Doveil et al., (1983). The Hamiltonian H_i in the vicinity of an island is renormalized relatively to the center of this island rather than to some global scaling constant, since the island width Δr is not very small compared to r for low m. The equations of motion for J_ψ, ψ now read

$$\dot{J}_\psi = -A_i \cos J_\psi \sin\psi \quad , \quad \dot{\psi} = -\delta + A_i \sin J_\psi \cos\psi \qquad (3)$$

where the variation of J_ψ expresses the oscillation of the perpendicular velocity $v_\perp$ around the average value $v_i = r_i\Omega_c/k_\perp$. Stable fixed points, the centers of stability islands in phase space, are defined by $\dot{J}_\psi = 0$, $\dot{\psi} = 0$ and appear for $J_\psi = 0$ (i.e., $I = I_i$ or $r = r_i$), $\psi = \cos^{-1}(\delta/A_i)$. The second equation has a solution only if $|\delta| < A_i$. This condition, namely that the wave frequency departure from a cyclotron harmonic be smaller than the normalized wave amplitude, signifies the emergence of islands in phase space and the breakdown of the linear theory. For $|\delta| \ll A_i$, Eq. (3) can be solved analytically yielding J, ψ as functions of the initial conditions and time. Ignoring δ, the system Eq. (3) can be written as

$$2\ddot{J} + A_i^2 \sin 2J = 0,$$

$$2\ddot{\psi} + A_i^2 \sin 2\psi = 0$$

where the subscript ψ is dropped from J_ψ. Both equations are coupled through the initial conditions and share the common invariant of the motion $W = 1/2(2\dot{J})^2 - A_i^2 \cos 2J = 1/2(2\dot{\psi})^2 - A_i^2 \cos 2\psi = A_i^2 - 2H_i^2$. One can then introduce a parameter λ by $\lambda^2 = 2A_i^2/(A_i^2 + W) = (1 - \cos^2 J \cos^2 \psi)^{-1}$ and solve Eq. (3) in terms of elliptic functions with the aid of the transformation $\sin J = \lambda^{-1} \sin \zeta$, $\sin \psi = \lambda^{-1} \sin \xi$. The solutions are

$$\begin{aligned} \sin J = \lambda^{-1} sn[F(\zeta, \lambda^{-1}), \lambda^{-1}] \quad , \quad \sin \psi = \lambda^{-1} sn[F(\xi, \lambda^{-1})\lambda^{-1}], \\ F(\zeta, \lambda^{-1}) = F(\zeta_0, \lambda^{-1}) + A_i t \quad , \quad F(\xi, \lambda^{-1}) = F(\xi_0, \lambda^{-1}) + A_i t, \end{aligned} \tag{4}$$

with $F(\xi, \lambda^{-1})$ the elliptic integral of the first kind. This result will now be used to compute the evolution of the particle velocity distribution function in time.

III. Computation of the Nonlinear Growth Rate

Let $\hat{f}(v_\perp;0)$ be the $v_\parallel$ averaged initial distribution function. Along the trajectories that are consistent with the existence of the wave $d\hat{f}/dt = 0$, so $\hat{f}(v_\perp(t);t) = \hat{f}[v_{\perp 0}(v_\perp(t),\vartheta(t);t);t=0]$. The rate of change of the kinetic energy density $dT/dt = N_0/V \int\int dXdYdz \int\int (1/2)dv_\perp^2 d\vartheta (1/2)mv_\perp^2 \partial\hat{f}/\partial t$, N_0=number density, can be written in the new normalized variables as

$$d\bar{T}/dt = N_0 \sum_{i=j}^{N} \sum_{j=0}^{2n-1} \int_{(j-1/2)\pi}^{(j+1/2)\pi} (d\psi/n) \int_{-\pi/2}^{\pi/2} dJ r_i (I_i + r_i J)(\partial \hat{f}_0/\partial I) I_i r_i \dot{J}_0(J,\psi) \qquad (5)$$

where use is made of the local variables around each fixed point r_i, $I = I_i + r_i J$, and $\hat{f}(v_\perp;t) = \hat{f}[I_0(I,\vartheta;t);t=0]$, $\partial\hat{f}/\partial t = \left(\partial\hat{f}(t=0)/\partial I_0\right)\dot{I}_0 \cong \left(\partial\hat{f}(t=0)/\partial I_0\right)_{I_i} r_i \dot{J}_0(J,\psi,t)$. The integration over J and ψ is carried up to the separatrices around each fixed point. They are given, from Eq. (3) with $\delta \ll A$, by the straight lines $J = \pm(\pi/2)$, $\psi = (j \pm 1/2)\pi$ corresponding to $r \cong r_i \pm \pi/2$, $\vartheta = j\pi/n$, $j = 0,\ldots,2n-1$ in Fig. 1. So for $\delta \ll A$ the size of the islands is essentially independent of A, $\Delta r \cong \pi$, and islands occupy all the available phase space. The summation over i stops at i=N that signifies the outermost island around the last fixed point r_n. For δ exactly zero N tends to ∞; however the main contribution comes from r_i less than few times the thermal velocity. The derivative of $\hat{f}$ is calculated at the center of the island $I_i = (1/2)r_i^2$ provided that the island width $\sim \pi$ is less than r_i. This still gives qualitatively correct behavior for the innermost islands with $r_i \sim \pi$. Using the equation of motion (3) for J, we substitute

$$\dot{J}_0(J,\psi) = -A_i \cos J_0(J(t),\psi(t)) \sin\psi_0(J(t),\psi(t))$$

into Eq. (5). Then, following the method of O'Neil (1965), equations (4) are inverted in time using the double angle formula for elliptic functions to obtain the expressions for $\cos J_0$, $\sin\psi_0$

$$\sin\psi_0 = (\sin\psi cn(z,\lambda^{-1})dn(z,\lambda^{-1}) - sn(z,\lambda^{-1})\sin J\cos^2\psi)/(1-\sin^2\psi sn^2(z,\lambda^{-1}))$$

$$\cos J_0 = (\cos J dn(z,\lambda^{-1}) - sn(z,\lambda^{-1})cn(z,\lambda^{-1})\sin J\cos J\sin\psi)/(1-\sin^2\psi sn^2(z,\lambda^{-1}))$$

After taking the product of the above expressions, all but one term will be averaged out during the integration in Eq. (5), with the remainder given by

$$\frac{dT}{dt} = \sum_{i=1}^{N} 8N_0 A_i r_i^3 \left(\frac{\partial \hat{f}_0}{\partial I_0}\right)_{I_i} \int_0^{\frac{\pi}{2}} d\psi \int_0^{\frac{\pi}{2}} dJ \frac{J \sin J \cos J sn(z,\lambda^{-1}) dn(z,\lambda^{-1})}{1 - \sin^2 J sn^2(z,\lambda^{-1})}.$$

The integrant $Z(J,\psi;z)$ (the ψ dependence is hidden in $\lambda(J,\psi)$) is Fourier transformed using the doubly periodic properties of the Jacobi functions in the complex plane,

$$Z(J,\psi;z) = 8 \sum_{m=0}^{\infty} \frac{2\pi J \sin J}{4K(\lambda^{-1})} \frac{q^{m+1/2}}{1+q^{2m+1}} \sin \frac{(2m+1)\pi F(\zeta,\lambda^{-1})}{2K(\lambda^{-1})} \sin \frac{(2m+1)\pi}{2K(\lambda^{-1})} z$$

$q = \exp[\pi K'(\lambda^{-1})/K(\lambda^{-1})]$, z=At, and $K(\lambda^{-1})$, $K'(\lambda^{-1})$ complete elliptic integrals of the first and second kind respectively. To compute $\int_0^{\pi/2}\int_0^{\pi/2} dJ d\psi Z(J,\psi;z)$, a change of variables from (J,ψ) to (J,λ) yields

$$\sum_{m=0}^{\infty} \int_1^{\infty} \frac{d\lambda}{\lambda(\lambda^2-1)^{1/2}} \int_0^{\sin^{-1}(\lambda^{-1})} dJ \frac{J \sin J}{[1-\lambda^2 \sin^2 J]^{1/2}} \frac{q^{m+1/2}}{K(\lambda^{-1})(1+q^{2m+1})}$$
$$\times \sin \frac{(2m+1)\pi F}{2K(\lambda^{-1})} \sin \frac{(2m+1)\pi}{2K(\lambda^{-1})} \mathrm{At}.$$

To integrate over J one can take advantage of the periodic properties of the elliptic functions by expressing J as $J = \cos^{-1}(dnF)$. The integral over dJ becomes

$$1/\lambda \int_0^K dF \cos^{-1}[dnF] \sin\left((2m+1)\pi F/2K(\lambda^{-1})\right) = 1/2 \ \mathrm{Im} \int_{-K}^{K} H(F) dF$$

with $H(F) = \lambda^{-1} \cos^{-1}[dnF] \exp[i(2m+1)\pi F/2K]$ analytic everywhere inside and on the contour of integration in Fig. 4 and obeying the following properties: $H(F+2K) = H(F)$, $H(F+2iK') = \{\pi snF \exp\left(i(2m+1)F\pi/2K'\right) - H(F)\} q^{-(2m+1)}$. Then,

$$\left(1+q^{-(2m+1)}\right) \int_{-K}^{K} H(F) dF =$$
$$q^{-(2m+1)} \left\{ -\int_{\sigma} H(F) dF + \pi \int_{-K}^{K} snF \exp[(2m+1)\pi F/(2K)] \right\}.$$

The path segment labeled by σ encircles the branch cut at $F = iK'$ since $\cos^{-1}[dnF] = -i\ell n[(i/\lambda) sn(iK'+\chi) + dn(iK'+\chi)] \cong -i\ell n(i\chi/2)$ around iK'. The contribution from

this part is computed by approximating $H(F)$ around iK' as

$$-i\int_\sigma (d\chi/\chi)\ell n[i\chi/2]\exp[i(2m+1)\pi\chi/2K(\kappa)]$$
$$= -i\lim_{p\to 0}\frac{d}{dp}\int_{\sigma'} d\eta \exp\left(-\left[(2m+1)\pi\eta/K(\kappa)\right]\right)/(-\eta)^{p+1}, \eta = -(i\chi/2).$$

Inside the right-hand side derivative is the well known Hankel integral, purely imaginary, thus $i\int_\sigma$ is pure real and does not contribute. Calculation of the remaining part of the integral leads to the final result in normalized units,

$$d\bar{T}/dt = -\sum_i 32\pi^3 N_0 A_i r_i^3 \left(\partial \hat{f}_0/\partial I\right)_{I_i} \sum_{m=0}^{\infty}\int_0^1 d\kappa c(\kappa,m)\sin[(2m+1)\pi A_i t/2K(\kappa)]$$

with

$$\kappa = \lambda^{-1}, c(\kappa,m) = (1-\kappa^2)^{-1/2} q^{-(2m+1)}/\left[(1+q^{2m+1})(1+q^{-(2m+1)})^2 K(\kappa)\right].$$

The quantity $c(\kappa,m)$ tends to zero at both ends of integration κ=0, κ=1 and the main contribution comes from particles away from the separatrix or the center of an island respectively, since $\dot{J}$ tends to zero there. Undoing the normalizations and equating $1/8\pi dE_0^2/dt = -dT/dt$ yields the evolution equation for the wave amplitude

$$\frac{dE_0}{dt} = \sum_{i=1}^{N}\Gamma^{(i)}\sum_{m=0}^{\infty}\int_0^1 d\kappa c(m,\kappa)\sin\frac{(2m+1)\pi A_i\Omega_c}{2K(\kappa)}t \qquad (6a)$$

$$\Gamma(i) = 32\pi^3\left(\frac{m\Omega_c^2}{k_\perp e}\right)\left(\frac{k_\perp\rho_i}{2\pi}\right)^{1/2} n\Omega_c\frac{\omega_{pi}^2\Omega_c}{k_\perp^3}\left(\frac{\partial \hat{f}_0}{\partial v_\perp}\right)_{v_\perp=\left(\frac{r_i\Omega_c}{k_\perp}\right)}. \qquad (6b)$$

The rate of change dE_0/dt given by Eq. (6a) is determined by the constants $\Gamma(i)$ in Eq. (6b), with the index i signifying the contribution from the i-th island chain in phase space, and is not proportional to E_0 as opposed to the usual exponential behavior during Landau damping. However, the damping rate is oscillating in time with a period proportional to the bouncing period of a particle around an island $\tau_b \sim 2\pi/A_i\Omega_c$ and therefore inversely proportional to the wave amplitude E_0. From Eq. (6b) dE_0/dt is negative for a monotonously decreasing velocity distribution of particles resulting in damping of the wave energy.

IV. Discussion and Implications

The damping is due to the fact that at any given moment, for an initially monotonously decreasing velocity distribution of particles there are more particles gaining energy from the wave than these losing energy to the wave. Although the above mechanism is the same as for the damping of electrostatic modes in unmagnetized plasma, there are some differences to be emphasized. The most obvious is that, for very short time intervals compared to the bouncing period τ_b, the damping rate is a constant independent of the wave amplitude E_0, as the right-hand side of Eq. (6a) is proportional to the constants $\Gamma(i)$ while E_0 enters only through the bouncing frequency $A_i(E_0)$. This is attributed to the fact that, because of a degeneracy in Hamiltonian Eq. (2), the width of the islands is independent of E_0, provided that $A_i \gg \delta$, and of order $\pi\Omega_c/k_\perp$, as opposed to $(2eE_0/mk_\perp)^{1/2}$ in the unmagnetized case. Thus the number of the trapped particles in each island entering the integral in the velocity space, Eq. (5), is independent of E_0. Actually, large size islands occupy most of the available phase space for arbitrary small E_0 as long as $\delta = \omega/\Omega_c - n$ can become much smaller than $A_i(E_0)$, Figs. 1,2. This produces a very effective mechanism coupling the wave energy directly to the bulk of the ions distribution function. For low harmonics $(n = 1, 2, \ldots)$ even cold particles $(k\rho_L < 1)$ can respond and be heated.

In the unmagnetized electrostatic case the width of the trapped particle island scales as the square root of the wave amplitude, thus particles crossing the amplitude dependent separatrices change from trapped to untrapped and vice versa and pose a serious difficulty in the analytic study of long time behavior. Here, however, the island width is insensitive to the wave amplitude A_i as long as $A_i \gg \delta \simeq 0$ and the main effect caused by the variation is a modification in the particle bouncing time $\tau_b = 2\pi/A_i\Omega$. Therefore it is the rate of change of the wave amplitude rather than the overall change that determines the time evolution and one can distinguish two cases depending on the relation between the particle bouncing time τ_b and the wave characteristic time $\tau_c^{-1} \sim d/dt\ell nE_0 \sim \Gamma/E_0$.

Case (a): $\tau_c \gg \tau_b$ occuring when $(2\pi/A\Omega_c)\,(\Gamma/E_0(0)) \sim \tau_b/\tau_c \ll 1$. The rate of change of the bouncing period τ_b is small compared to the bouncing period itself. Thus, the solutions (4) are assumed to be valid with the constant A_i replaced by $A_i(t)$ in the spirit of the WKB approximation. This is verified numerically by the results in Fig. 5

where the trajectories shown correspond to the case of a slowly varying wave amplitude $A(t) = A_0 e^{-wt}$ with $\tau_c \cong w^{-1} \gg \tau_b$. They are very similar to the trajectories with constant A plotted in Fig. 1 while the time span plotted is $2.25\tau_c$.

Equation (6a) can now be solved exactly using $A_i(t) = \varepsilon_i E_0(t)$ with $\varepsilon_i = (e2^{3/2}k_\perp)/(m\Omega_c^2 r_i^{3/2})$, obtained by combining Eqs. (2a) and (2b). The solution $E_0(t)$ is given in implicit form by

$$E_0(t) = E_0(0)\Bigg\{1 - \sum_{i=1}^{\infty} \frac{\Gamma(i)}{\varepsilon_i \Omega_c E_0^2(0)} \sum_{m=0}^{\infty} \int_0^1 d\kappa c(\kappa, m) \times [K(\kappa)/(2m+1)\pi]\,[1 - \cos(\beta_i(\kappa, m)E_0(t)t)]\Bigg\}^{1/2} \tag{7}$$

with

$$\beta_i(\kappa, m) = \frac{\varepsilon_i \pi (2m+1)\Omega_c}{2K(\kappa)}$$

and $c(\kappa, m)$ rewritten as

$$c(\kappa, m) = \frac{1}{4}\frac{1 - \tanh u_m}{1 + \cosh u_m}\frac{1}{\sqrt{1-\kappa^2}K(\kappa)} \quad , \quad u_m = (2m+1)\frac{\pi K'(\kappa)}{2K(\kappa)}.$$

The long time limit can now be taken, $t \gg \tau_c$, and the above complicated Eq. (7) reduces to a simple form. As the time t increases, the cosine terms in Eq. (7) oscillate with an ever increasing frequency over the slowly varying $c(\kappa, m)$ and the integral over κ goes to zero as $t \to \infty$. Thus

$$E_\infty \equiv E_0(t \to \infty) \cong E_0(0)\left[1 - \frac{1}{2}\sum_{i=1}^{N} \frac{\Gamma(i)}{\varepsilon_i \Omega_c E_0^2(0)} \sum_{m}^{\infty} \int_0^{1-\rho} d\kappa \frac{c(\kappa, m)}{\beta_i(\kappa, m)}\right]^{1/2}. \tag{8}$$

where $\rho \ll 1$ in the upper limit of the integration takes care of the finite width of the stochastic layer around a separatrix (Fukuyama et al., 1977). In short the behavior of $E_0(t)$ is that of an incoherent oscillation around an ever diminishing value tending asymptotically to $E_\infty \sim E_0(0)(1 - \tau_b/\tau_c)$ while the distribution function tends simultaneously to a state of collisionless equilibrium with the wave such that f_∞ is constant along the trajectories $H_i = c$, $f_\infty \to f(H_i)$ with H_i given by Eq. (2b) (see Figs. 1 and 6(d)). The depletion of the electrostatic energy stored in the initial field must balance the difference

in kinetic energy ΔT_∞ between the initial Maxwellian and the final equilibrium state, thus $(1/4\pi)E^2(0)(\tau_b/\tau_c) = \Delta T_\infty$. Since ΔT_∞ is independent of the wave amplitude, $E_0(0)$ must be above a certain threshold, otherwise $A_i(t)t$ will remain small as $t \to \infty$ and the long time limit of Eq. (7) is not given by Eq. (8). The case of relatively small energy transfer compared to the initial electrostatic energy described by Eq. (8) results from solving an initial value problem. The situation is different for the boundary value problem appropriate for rf heating where the depletion of the electrostatic energy is balanced by the power influx provided by an antenna. Then a quasi-steady situation can be reached with the amplitude of the electric field remaining practically constant while particle heating continues, no matter how small τ_b/τ_c or $E_0(0)$ is, until the final stage with the multiflattened velocity distribution is reached. Some numerical results for this case are given later in this section.

Case (b): $\tau_c \lesssim \tau_b$ occuring when $(2\pi/\Omega_c A)\ (\Gamma/E_0(0)) \gtrsim 1$. In that case, even if the overall change $\Delta E(t)/E_0(0)$ turns out to be small, $A(t)$ changes with a rate comparable to the bouncing frequency and new resonances may appear changing the motion considerably. The substitution $A(t)$ in place of constant A works only for time $t \ll \tau_c \lesssim \tau_b$ or $At \ll 1$. Then a linear expansion of the sine term in Eq. (6a) yields

$$dE_0/dt = E_0\gamma' t$$

with

$$\gamma' = 32\pi^3 n^2(\omega_p^2\Omega_c/k_\perp^3)\sum_i(\Omega_c^2/k_\perp\rho_i)(\partial\hat{f}/\partial v_\perp)_{v_i}\sum_m(2m+1)\int_0^1 d\kappa c(\kappa,m)/2K(\kappa), \quad (9)$$

so the short time behavior becomes exponential with $E_0(t) \cong E_0(0)\exp[\gamma' t^2/2]$.

The dependence of the trapped particle bouncing frequency on the particle velocity causes phase mixing that results in a flattening of the velocity distribution function around the center of an island in phase space. In the unmagnetized case, studied in detail (O'Neil 1965), there is a single island in the interval $-\infty < v_z < +\infty$, $0 < k_\parallel z < 2\pi$ and a single plateau is formed on $f(v_z)$ centered around $v_z = \omega/k_\parallel$. Here a sequence of plateaus is being developed in $f(v_\perp)$, each one centered around $v_\perp = v_i$, where v_i is the center of the i-th chain of islands given by the i-th zero of $J_n'(k_\perp v_\perp/\Omega_c) = 0$.

To demonstrate the validity of the theory, a series of numerical simulations is peformed using a $1-1/2$ dimensional self-consistent electrostatic particle code to model a uniformly magnetized plasma. The "multiflattening" of the distribution function is evident from the typical numerical results in Figs. 6(a)-6(d) showing the time evolution of the initial Maxwellian distribution. The Bernstein wave is driven externally at frequency $\omega = 2\Omega_c$ across the magnetic field. In the dimensionless code parameters with time normalized to ω_p^{-1}, velocities to $\omega_p \Delta$ (so that $\Delta = \lambda_D$ for $v_{th} = 1$) the cyclotron frequency wave is set to $\Omega_c = 0.125$ and $k_\perp = 0.295$ while the wave amplitude E_0 (in units $\omega_p^2 \Delta \frac{m}{e}$) is remaining practically constant near $E_0 \simeq 0.06$ after a short initial build-up stage. The corresponding bouncing periods for the three innermost islands are therefore $\tau_{1b} = 68\omega_p^{-1}$, $\tau_{2b} = 245\omega_p^{-1}$ and $\tau_{3b} = 1130\omega_p^{-1}$. The initial Maxwellian distribution of 153,600 particles with $k_\perp \rho_{th} \cong 6$, Fig. 6(a), evolves into the multiflattened one in Fig. 6(d). The three plateaus in 6(d) are formed around the centers of trapped particle islands (Fig. 1) given by the zeros of $J_2'(k_\perp \rho_L)$ at approximately $(k\rho_L)^2 = 10$, 45 and 99 respectively. Steep gradients are built at the positions of the separatrices, zeros of $J_2(k_\perp \rho)$ at approximately $(k\rho_L)^2 = 26$, 71 and 135. Some diffusion across the separatrices due to statistical noise is inevitable although the wave amplitude remained below the stochasticity threshold. The time succession of the plateau formation agrees with the theory as the mixing time τ_m is proportional to the bouncing period, inversely proportional to the normalized amplitude, $\tau_m \sim 2\pi/A_i \propto (k\rho_L)^{3/2}$, Eq. (2b). Thus the innermost island phase mixes first, Fig. 1(b) followed by the second and third islands in 6(c) and 6(d) respectively.

The time history of the kinetic energy during the same run is shown in Fig. 7. After a short initial state of slow growth due to the sinusoidal time dependence of the energy absorption rate, the growth remains almost linear until the final saturation state of slow growth is reached. From the slope of the linear part it is found that $\tau_{ck} \equiv (d/dt)\ell nT \sim 5 \times 10^3 \omega_{pi}^{-1}$ much larger than the bouncing time τ_b for all three island chains. Recalling that Eq. (6a) was obtained from the expression for the kinetic energy growth rate by setting $dT/dt = -(1/4\pi)E_0(dE_0/dt)$, one can obtain an order of magnitude estimate for the theoretically predicted growth by converting the quantities in Eq. (6a) into the numerical simulation scaling, considering only the m=0 time harmonic and assuming that the rest

harmonics give a correction $C \sim 0(1)$. It is found that $\tau_{th} \sim C^{-1} \times 1.2 \times 10^4$, thus the numerically observed growth rate exceeds the theoretical by a factor of 2. The difference can be partly attributed to diffusion across the sharp distribution gradients built near the separatrices due to statistical noise and the intrinsic stochastic layer around each island (note the slow smoothing of the "steps" in the distribution function, Fig. (6e) and the small but persistent growth of the kinetic energy at the end of the run, Fig. 7).

The long time phase mixing of the distribution function coincides with the phase mixing of $dE_0/dt \to 0$ as $t \to \infty$ and a final state of dynamic equilibrium between the wave and the distribution function is reached asymptotically. The evolution towards this final state can stop however if it so happens that the wave amplitude $E_0(t)$ drops below the threshold for particle trapping, i.e., $\varepsilon_i E_0(t) < A_{th} \cong \delta$. Past that time the linear undamped behavior of Eqs. (1) is recovered. On the other hand for very large initial $E_0(0)$, the coherent motion in Figs. 1,2 is replaced by stochastic diffusion (Hsu 1982). The innermost islands disappear first and the stochastic regime is spreading towards larger $v_\perp$ for increasing A_i. The results obtained so far for $k_\| = 0$ are approximately correct for small but finite $k_\|$ as long as the Doppler frequency shift from the cyclotron harmonic $\delta' = k_\| v_{th}/\Omega_c$ does not violate the perpendicular trapping condition $\delta' < A$ or $k_\|/k_\perp < eE_0 J_n'(k_\perp \rho_L)/(2k_\perp m v_{th}^2)$. The results in this paper can be easily extended to apply for the general case of an almost perpendicular electrostatic mode near an ion cyclotron harmonic. In particular they can be important in understanding the observed ion heating through the fast magnetosonic wave in two ion species plasmas. For small minority ion concentration, the fast magnetosonic mode is converted to a perpendicular electrostatic mode close to the ion-ion hybrid resonance layer (Swanson 1975), with frequency near the minority ion cyclotron frequency, thus perpendicular trapping can be the heat absorption mechanism in case of small $k_\|$, since the standard linear Landau damping of ions due to $k_\|$, Eq. (1), is insufficient to account for significant ion heating.

In conclusion, the damping of a single perpendicular monochromatic Bernstein mode due to non-linear particle trapping by the wave has been examined. Perhaps, to avoid confusion, it should be mentioned here that the situation considered in this paper is completely different from the one studied theoretically by Baldwin and Rolands (1966)

and numerically by Kamimura, Wagner and Dawson (1978). The damping in their case is a collective effect coming from the linear superposition of infinitely many, closely spaced, Bernstein modes at the limit when the frequency separation between successive cyclotron harmonics tends to zero, i.e., the magnetic field vanishes. Each mode by itself is undamped with a dispersion relation of the form of Eqs. (1), based on unperturbed cyclotron orbits. However, for small but finite ω_c, the collective damping exists for only a short time compared to Ω_c^{-1} while for times $t_n \sim 2\pi n/\Omega_c$ the system exhibits semiperiodic behavior and returns to the initial state.

Acknowledgements

The author wants to thank J.D. Meiss and R. Carrera for many helpful discussions as well as J. Leboeuf for providing the particle code. This work was supported by the U.S. Department of Energy Grant #DE-FG05-80ET-53088.

References

BALDWIN, D.E. and ROWLANDS, G. 1966, Phys. Fluids **9**, 2444.

DOVEIL, F. and MENDONCA, J.T., 1983, Phys. Fluids **26**, 3279.

FUKUYAMA, A., MOMOTA H., ITATANI R., and TAKIZUKA T. 1977, Phys. Rev. Lett. **38**, 701.

HSU, J.Y. 1982, Phys. Fluids **25**, 159.

KAMIMURA T., WAGNER T., and DAWSON J.M. 1978, Phys. Fluids **21**, 1151.

KARNEY, C.F.F. 1978, Phys. Fluids **21**, 1584.

O'NEIL T. 1965, Phys. Fluids **8**, 2255.

SWANSON D.G. 1975, Phys. Rev. Lett. **36**, 316.

Figure Captions

1. Trajectories in phase space showing $r=k_\perp \rho_L$ versus $\vartheta = \Omega_c t$ for different particles and for $\nu = \omega/\Omega_c = 2.00$, $0.0034 \leq A_i \leq 0.0360$, $\delta=0$. Each trajectory is obtained by numerically integrating the equations of motion for the single particle Hamiltonian, Eq. (2a).
2. Same as Fig. 1 with $\nu = 2.006$, $0.162 \leq A_i \leq 0.015$, $\Delta = 0.006 \leq A_i$.
3. Same as Fig. 1 with $\nu = 1.93$, $A_i \leq 0.04$. Here $|\delta| = 0.07 > A_i$.
4. Contour of integration for $H(F)$.
5. Same as in Fig. 1 with slowly varying amplitude $A_i(t) = A_i e^{-wt}$, $w = 0.001$.
6. Plot of $f(v_\perp)$ versus $(k_\perp \rho_L)^2$ at times (a) t=0, (b) t=$183\omega_p^{-1}$, (c) t=$244\omega_p^{-1}$ (d) t=$366\omega_p^{-1}$, (e) t=$549\omega_p^{-1}$. Dotted line in (b)-(e) represents the initial distribution. The results are created by using a self-consistent electrostatic particle code to model a uniformly magnetized plasma.
7. Kinetic energy as a function of time for the run shown in Fig. 6.

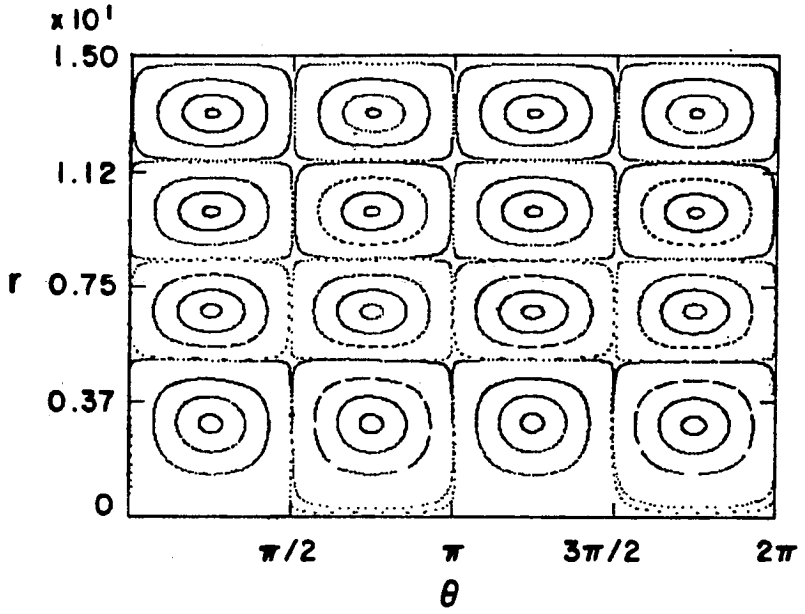

FIG. 1

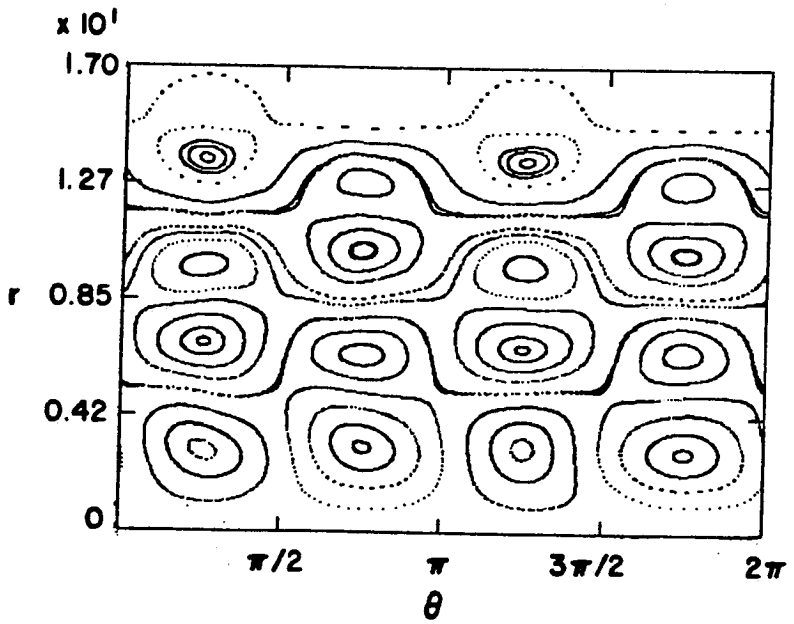

FIG. 2

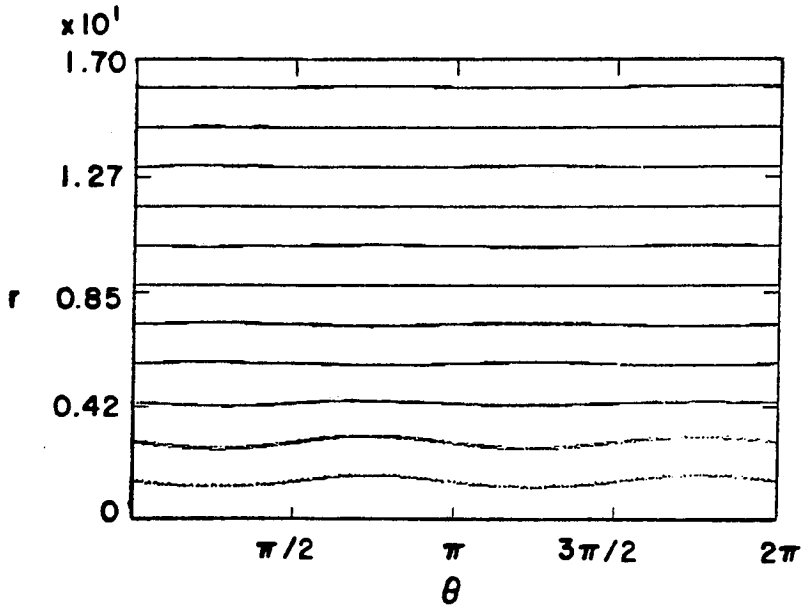

FIG. 3

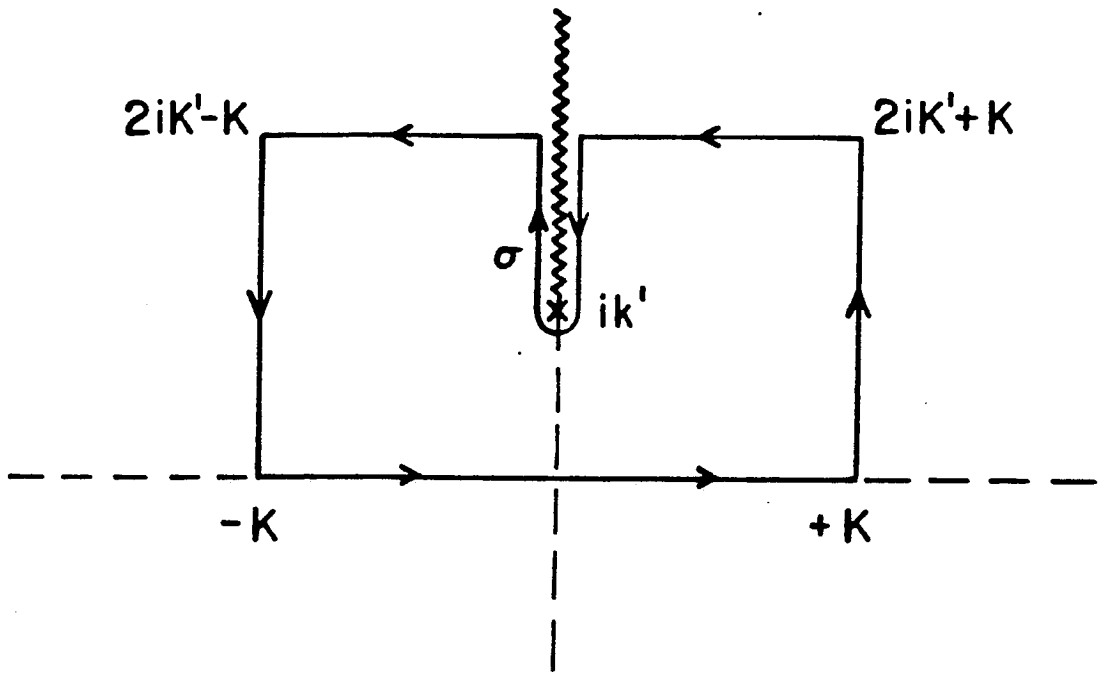

FIG. 4

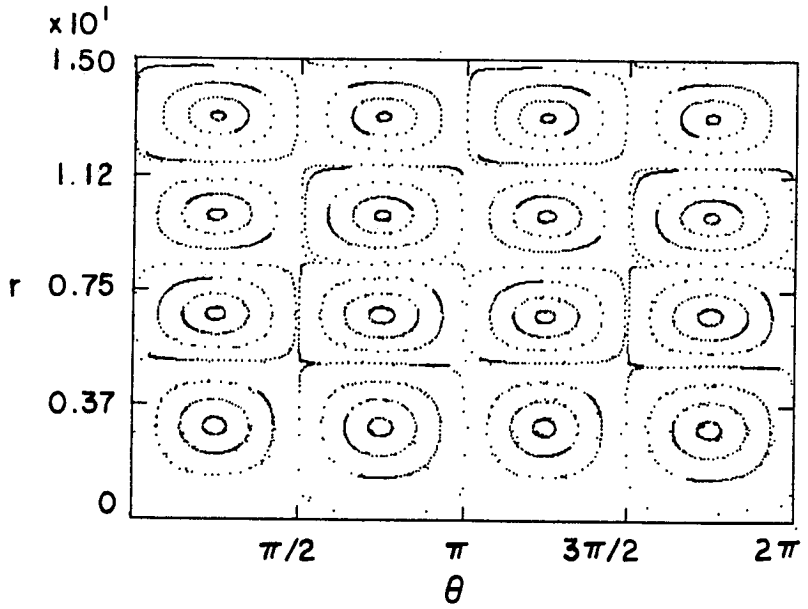

FIG. 5

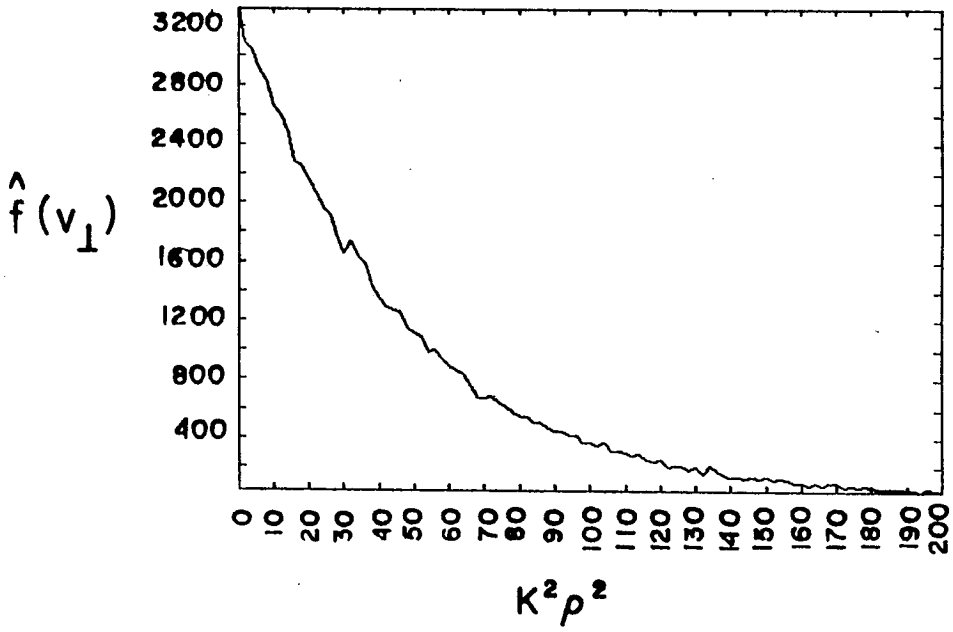
$\hat{f}(v_\perp)$
3200
2800
2400
2000
1600
1200
800
400
0
10
20
30
40
50
60
70
80
90
100
110
120
130
140
150
160
170
180
190
200
$K^2\rho^2$

FIG. 6(a)

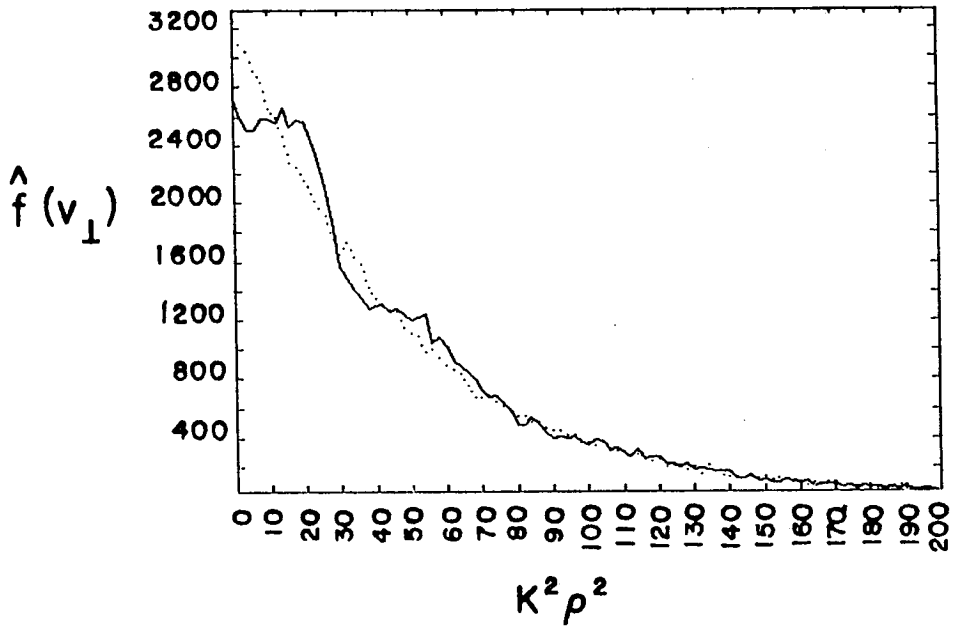
3200
2800
2400
2000
1600
1200
800
400
$\hat{f}(v_\perp)$
0 10 20 30 40 50 60 70 80 90 100 110 120 130 140 150 160 170 180 190 200
$K^2\rho^2$

FIG. 6(b)

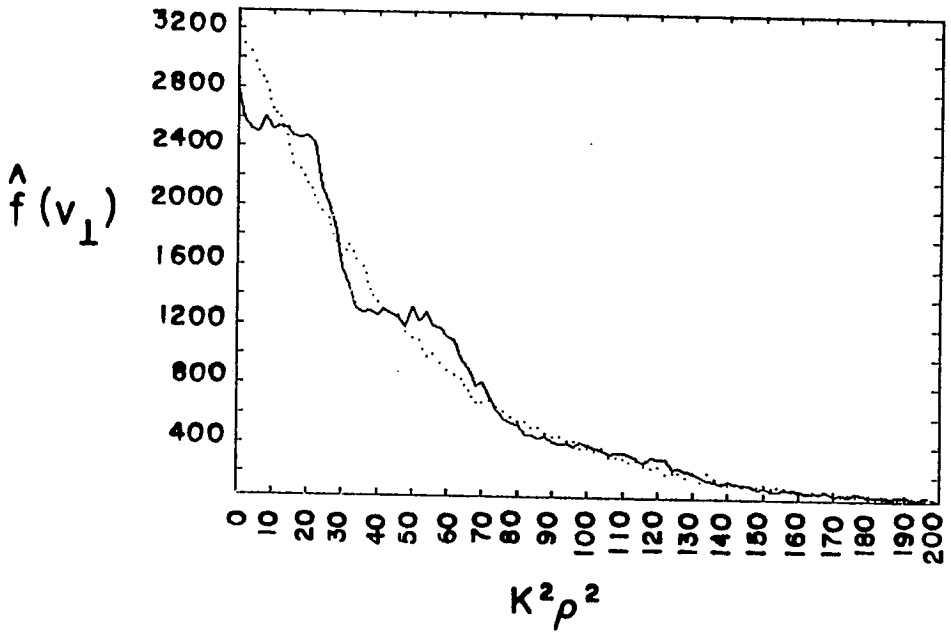
3200
2800
2400
2000
1600
1200
800
400
$\hat{f}(v_\perp)$
0 10 20 30 40 50 60 70 80 90 100 110 120 130 140 150 160 170 180 190 200
$K^2\rho^2$

FIG. 6(c)

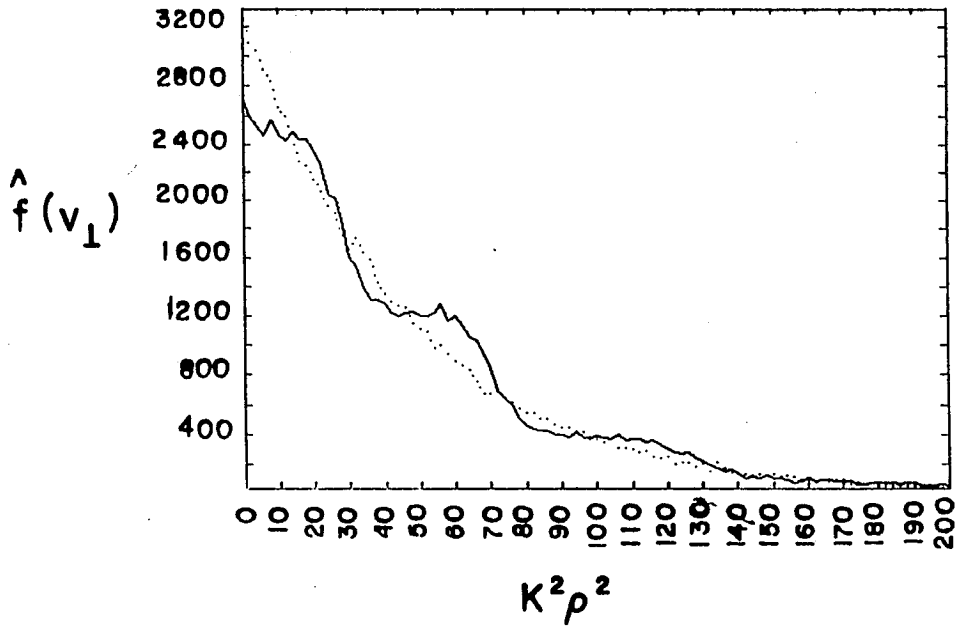
3200
2800
2400
2000
1600
1200
800
400
$\hat{f}(v_\perp)$
0 10 20 30 40 50 60 70 80 90 100 110 120 130 140 150 160 170 180 190 200
$K^2\rho^2$

FIG. 6(d)

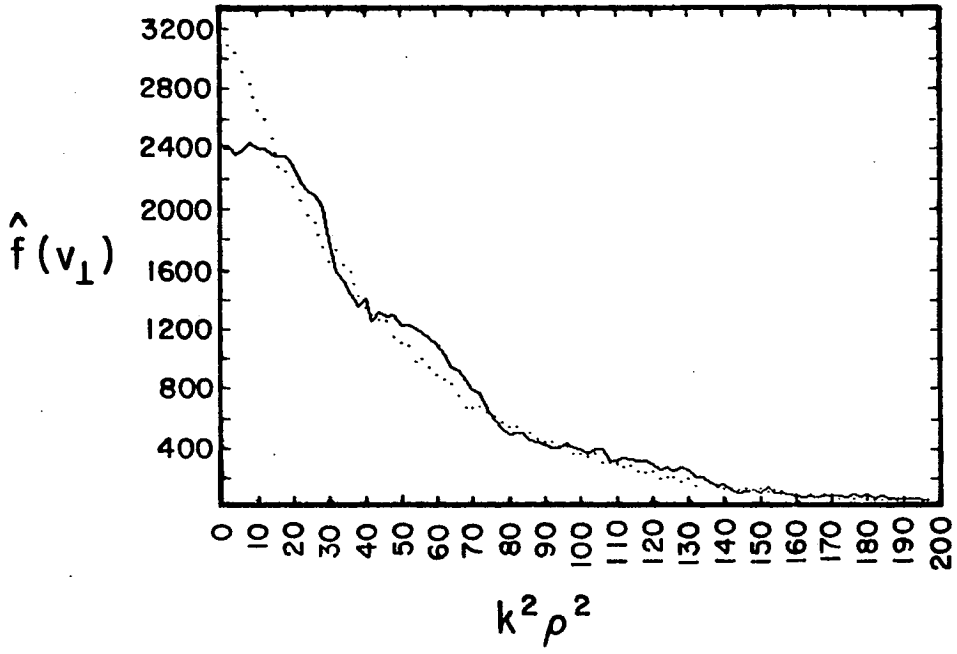
3200
2800
2400
2000
1600
1200
800
400
$\hat{f}(v_\perp)$
0 10 20 30 40 50 60 70 80 90 100 110 120 130 140 150 160 170 180 190 200
$k^2\rho^2$

FIG. 6(e)

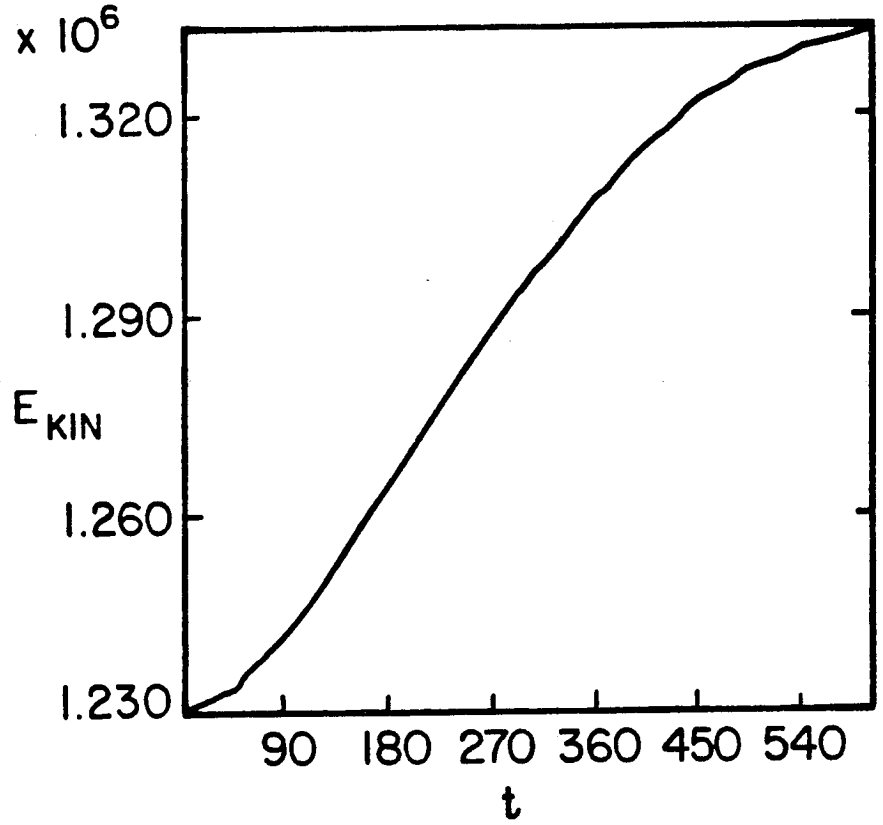

FIG. 7